A MULTIVARIABLE OPTIMAL ENERGY MANAGEMENT STRATEGY FOR STANDALONE DC MICROGRIDS

G.Sandhyarani 1, SK.Shakir Hussain 2

1M.Tech Student, Anu Bose Institute of Technology, Paloncha, khammam, Telangana, India 2Assoc Prof Dept of EEE, Anu Bose Institute of Technology, Paloncha, khammam, Telangana, India

Abstract—Due to substantial generation and demand fluctuations in standalone green microgrids, energy management strategies are becoming essential for the power sharing and voltage regulation purposes. The classical energy management strategies employ the maximum power point tracking (MPPT) algorithms and rely on batteries in case of possible excess or deficit of energy. However, in order to realize constant current-constant voltage (IU) charging regime and increase the life span of batteries, energy management strategies require being more flexible with the power curtailment feature. In this paper, a coordinated and multivariable energy management strategy is proposed that employs a wind turbine and a photovoltaic array of a standalone DC microgrid as controllable generators by adjusting the pitch angle and the switching duty cycles. The proposed strategy is developed as an online nonlinear model predictive control (NMPC) algorithm. Applying to a sample standalone dc microgrid, the developed controller realizes the IU regime for charging the battery bank. The variable load demands are also shared accurately between generators in proportion to their ratings. Moreover, the DC bus voltage is regulated within a predefined range, as a design parameter.

I. INTRODUCTION

The near future distribution networks will consist of several interconnected microgrids that will locally generate, consume, and store energy [1]. A microgrid may operate as an extension of the main grid, i.e., grid-connected, or as a standalone network with no connection to the grid. Standalone de microgrids have some distinct applications in avionic, automotive, or marine industries, as well as remote rural areas. While ac systems suffer from the need of synchronization of several generators [2], [3], de microgrids are more efficient due to the fact that de generators and storages do not need ac-de converters for being connected to de microgrids [4], [1]. The three well-known issues regarding voltage regulation, power sharing, and battery management, are more severe in standalone green

microgrids, that comprise of just discontinuous sun oriented and wind energysources, and lead to the need of more complex controlstrategies. The solidness of a dc microgrid is measured as far as the stability of its dc transport voltage level [5], [6], which is one of the primary control targets [7]. The framework voltage source converter (G-VSCs) are the

essential slack terminals to regulatethe voltage level of matrix associated microgrids (e.g., [5], [6], [8], [9]). Battery banks, then again, are compelling slackterminals for standalone microgrids [6]; in any case, their energyabsorbing limits are restricted with respect to various operational constraints, as clarified later in this area. All together tregulate the voltage level of standalone dc microgrids, the worksin [2] and [6] present burden shedding systems for the cases inwhich there is deficient force era or vitality storage. The works in [10]-[12], then again, introduce strategiesthat diminish the renewable force eras of standalone dmicrogrids if the battery bank can't retain the abundance generation. These shortening techniques confine the batteries charginrate by the greatest engrossing force; in any case, the maximumcharging current should likewise be restricted. Besides, they do notcurtail the force of every generator in extent to its rating. In request to forestall over-focusing on conditions and circulating currents between generators [13], load requests need to be shared between every single slack Dg in extent to theiratings[7], [14]. The works in [3], [7], [13], and [15]–[18] extentle traditional hang control strategy [11] for dc slackterminals by supplanting the ordinary bends with eithera dc power-dc voltage or a dc voltage-yield current curve. However, standalone dc microgrids are normally found insmall-scale zones where the force sharing between DGs can be overseen by unified calculations which are less influenced bytwo issues: 1) batteries in charging mode are nonlinear loadscausing contortions to the framework voltage; and 2) the absolutevoltage level of a standalone microgrid is moved as the consequence of the heap request variation.A number of marvels influence the batteries operation amid the charging mode [19]: 1) applying high charging streams, the batteries voltages rapidly reach to the gassing threshold;2) the inward resistor and subsequently control misfortunes and warm impacts increment at high SOC levels; and 3) batteries can't befully accused of a steady high charging current. The work in [6] limits, as an operational imperative, the most extreme absorbe influence by the batteries keeping in mind the end goal to shield them from being cheated. Nonetheless, since batteries go about as nonlinear burdens amid the charging mode, it doesn't as a matter of course farthest point the charging currents. On the other hand, the works in [10] limits the maximumattainable SOC that prompts unused capacities. Depending on the extent of the force era to the load request proportion inside standalone DC microgrids, three casesare imagined: 1) power era and burden interest are balanced;2) load request surpasses power era causes dc transport voltage to drop without any heap shedding; and 3) powergeneration is higher than burden request drives batteries to be overchargedand transport voltage to climb. This study concentrates on case 3 in which the created power must be shortened on the off chance that it violatesthe batteries charging rates or if batteries are completely charged. A novel vitality administration system (EMS) is proposed to address, as its control goals, three previously mentioned issues comparing standalone dc microgrids; i.e., dc transport regulation, proportional power sharing, and battery administration. Rather than the procedures accessible in writing in which renewableenergy frameworks (RESs) dependably work in their MPPT mode, the proposed multivariable technique utilizes a wind turbine and a PV exhibit as controllable generators and reduces their generationsif it is fundamental. The proposed EMS is produced as an online novel NMPC methodology that persistently takes care of an optimalcontrol issue (OCP) and finds the ideal qualities of the pitch point and three exchanging obligation cycles. It all the while controls four variables of microgrids: 1) power coefficient of the wind turbine; 2) rakish speed of the wind generator; 3) working voltage of the PV exhibit; and 4) charging current of the battery bank. It is demonstrated that, utilizing new accessible nonlinear advancement procedures and instruments, the computational timeto understand the subsequent NMPC methodology is in passable extent. Dissimilar to dump load-based systems that exclusive secure the batteryfromovercharging, the proposed procedure executes the IU charging administration that expands the batteries life range. Also, evacuating dump stacks, the general establishment expense is reduced. This paper is sorted out as takes after: Section II presentsthe numerical model of standalone dc microgrids. Area III demonstrates the exhibited EMS as an OCP issue which is acknowledged as a NMPC-based procedure. Segment IV presents and discusses the got comes about. At long last, the finish of the study is given in Section V.

II. SYSTEM DESCRIPTIONS AND MODELING

The standalone dc microgrid in Fig. 1 is a small scale microgrid for remote applications. The wind turbine operates at variablespeeds and is connected to the electrical generator directly, i.e., the direct-drive coupling. The variable speed

operation is more flexible for the power management and MPPT applications[21]. Furthermore, direct-drive coupling is more efficient and reliable and is more popular for small-scale wind turbines [22]. In spite of high cost, permanent magnet synchronous generators(PMSGs) are the most dominant type of direct-drive generators in the market [22], chiefly due to higher efficiency. From Fig. 1, it can be seen that battery bank is connected to the dc bus through a dc-coupled structure, i.e., via a dc-dcconverter, which is more flexible in terms of implementing differentcharging and discharging regimes despite more power losses [19].

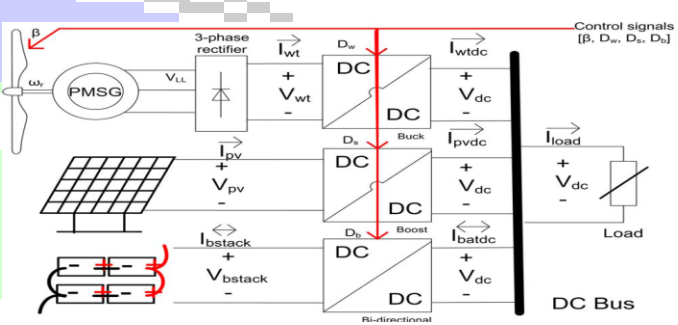


Fig. 1. Topology of a small-scale and standalone dc microgrid.

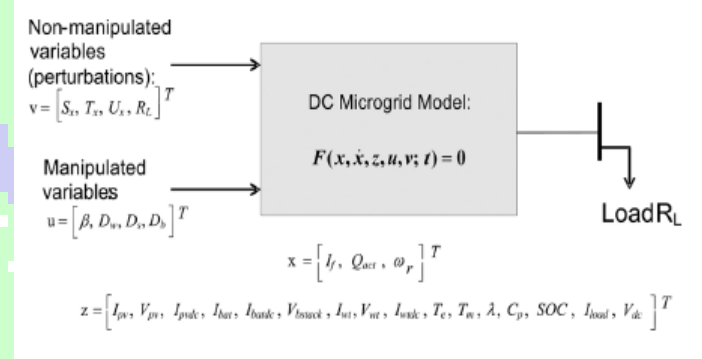


Fig. 2. Modified version of the system model in [20] for this paper.

The authors in [20] presented a mathematical model of standalonegreen dc microgrids as hybrid differential algebraic equations(hybrid DAEs). Fig. 2 summarizes a modified version of the proposed model in [20].

Since this paper focuses on the case in which there is an excess power greater than or equal to the maximum possible absorbing rate of the battery bank, thehybrid nature of the battery bank operation is ignored for the sake of simplicity. The differential and algebraic states, i.e., and , and the manipulated and non-manipulated control variables, namely, and , are detailed later throughout the next subsections.

In what follows, the following notations are used to model the standalone dc microgrid in Fig. 1 as DAEs:

$$\mathcal{F}(\mathbf{x}, \dot{\mathbf{x}}, \mathbf{z}, \mathbf{u}, \mathbf{v}) = \begin{bmatrix} f_1(\mathbf{x}, \dot{\mathbf{x}}, \mathbf{z}, \mathbf{u}, \mathbf{v}) \\ f_2(\mathbf{x}, \dot{\mathbf{x}}, \mathbf{z}, \mathbf{u}, \mathbf{v}) \\ \vdots \\ f_{24}(\mathbf{x}, \dot{\mathbf{x}}, \mathbf{z}, \mathbf{u}, \mathbf{v}) \end{bmatrix} = 0 \tag{1}$$

where \mathcal{F} is a set of implicit differential and algebraic functionals f_i for $i \in \{1, 2, ..., 24\}$.

The first two constraints f_1 and f_2 are due to the fact that in standalone de microgrids the sum of the generated, stored, and consumed powers is always zero:

$$f_1 = V_{dc} \left(I_{pvdc} + I_{wtdc} + I_{batdc} - I_{load} \right), \tag{2a}$$

$$f_2 = V_{dc} - I_{load}R_L. (2b)$$

A. Wind Branch:

Performance of the wind turbines is measured a the power coefficient curve with respect to the tip speed ratio and pitch angle [23]. Equation (3) shows the power coefficient curve of three-blade wind turbines [24]:

$$f_3 = C_{p,norm} - \frac{1}{C_{p,max}} \times$$

$$(C_1(\frac{C_2}{\lambda_i} - C_3\beta - C_4) \exp(-\frac{C_5}{\lambda_i}) + C_6\lambda), \quad (3a)$$

$$f_4 = \lambda - \frac{Rad \times \omega_r}{U_r},\tag{3b}$$

$$f_5 = \lambda_i - \left(\frac{1}{\lambda + 0.08\beta} - \frac{0.035}{\beta^3 + 1}\right)^{-1},$$
 (3c)

where λ and β , respectively, are the tip speed ratio and pitch angle. Rad is the radius of the blades and $C_{p,\text{max}}$ is the maximum achievable power coefficient at the optimum tip speed ratio of λ_{opt} [24]. The experimental coefficients $C_1 - C_6$ are defined in Table II and λ_i is an intermediate variable.

Equation (4) presents the connected PMSG generator:

$$f_6 = \frac{\mathrm{d}\omega_r}{\mathrm{d}t}(t) - \frac{1}{J}(T_e - T_m - F\omega_r), \tag{4a}$$

$$f_7 = -T_e \times \omega_r - I_{wtdc} \times V_{dc}, \tag{4b}$$

$$f_7 = -T_e \times \omega_r - I_{wtdc} \times V_{dc},$$

$$f_8 = -T_m \times \omega_r - (C_{p,norm}(\frac{U_x}{U_{r,hood}})^3 P_{nom}.$$
(4e)

Energy management strategies of microgrids must estimate the dc bus voltage level deviation from its set point in about every 5–10 s [13]. It means that except the angular velocity of the generator (4a) all other fast voltage and current dynamics can be ignored. It is also assumed that there is no mechanical and electrical losses through the powertrain and therefore theelectromagnetic power given by (4b) is equal to the output electrical power of the wind branch. Equation (4c) shows that the PMSG is connected directly to turbine, which rotates at low speed, and therefore needs to havemultiple pole pairs [22]. Hence, the electrical frequency is times faster than the mechanical angular velocity . The shaftinertia and the combined viscous friction coefficientof PMSG are given by the manufacturers. For energy management strategies, the average model of the buck converter is replaced with the steady-state equations for the continuous conduction mode (CCM) [25]:

$$f_9 = V_{dc} - D_w V_{wt}, \tag{5a}$$

$$f_{10} = I_{wt} - D_w I_{wtdc} \tag{5b}$$

where D_w is the switching duty cycle of the converter and all remaining parameters are as depicted in Fig. 1.

The average dc output voltage of the rectifier, V_{wt} , in presence of the non-instantaneous current commutation is calculated as follows [25]:

$$V_{wt} = 1.35V_{LL} - \frac{3}{\pi}\omega_e L_s I_{wt} \tag{6}$$

where having the number of the pole pairs P and the flux linkage ψ (V.s) (see Table II) and replacing V_{LL} , i.e., the r.m.s. value of the line-to-line output voltage of the generator, with

 $\sqrt{3/2}P\psi\omega_r$, one calculates the dc output current of the wind branch, I_{wtdc} , as follows:

$$f_{11} = I_{wtdc} - \frac{\pi}{3P\omega_r L_s D_w} \left\{ \frac{1.35\sqrt{3}P\psi\omega_r}{\sqrt{2}} - \frac{V_{dc}}{D_w} \right\}.$$
 (7)

B. Battery Branch

The charging operation of a lead acid battery bank, consisting of $N_{batp} \times N_{bats}$ batteries, is modeled as (8) [26]:

$$\begin{split} f_{12} &= \frac{V_{bstack}}{N_{bats}} - V_0 + R_{bat} \frac{I_{bstack}}{N_{batp}} + \\ &= \frac{P_1 C_{\max}}{C_{\max} - Q_{act}} Q_{act} + \frac{P_1 C_{\max}}{Q_{act} + 0.1 C_{\max}} I_f, \quad \text{(8a)} \end{split}$$

$$f_{13} = \frac{\mathrm{d}Q_{act}}{\mathrm{d}t}(t) - \frac{1}{3600} \frac{I_{bstack}(t)}{N_{batp}},$$
 (8b)

$$f_{14} = \frac{\mathrm{d}I_f}{\mathrm{d}t}(t) + \frac{1}{T_s} \left(I_f - \frac{I_{bstack}}{N_{batp}}\right),\tag{8c}$$

$$f_{15} = V_{bstack} - \frac{V_{dc}}{1 - D_b},\tag{8d}$$

$$f_{16} = I_{bstack} - (1 - D_b)I_{batdc}, \tag{8e}$$

$$f_{17} = SOC - \left\{1 - \frac{Q_{act}}{C_{\text{max}}}\right\} \tag{8f}$$

where, , and are, respectively, the voltage, current, and state of charge of the battery bank. is the filtered value of the battery

current with the time constant of and is the actual battery capacity. The experimental parameter requires being identified for each type of battery while the maximum amount of the battery capacity, , internal resistorof battery, , and the battery constant voltage, , are given by manufacturers (see Table II). By ignoring the discharging mode of the battery bank operation, the bi-directional converter acts as a boost-type converter [(8d)–(8e)].

C. Solar Branch

The equivalent electrical circuit of the PV module [27], [28] mis used to mathematically model the solar branch, consisting of a PV array and a boost converter [29]. Eq. (9) shows the characteristic equations of a PV array, consisting of PV modules:

$$\begin{split} f_{18} &= I_{pv} - I_{ph} + \\ &I_{0} \left\{ \exp(\frac{V_{pv} + \frac{N_{pvs}}{N_{pvp}} R_{s} I_{pv}}{n_{d} N_{s}} \frac{q \times N_{pvs}}{K T_{c}}) - 1 \right\} + \\ &\frac{V_{pv} + \frac{N_{pvs}}{N_{pvp}} R_{s} I_{pv}}{\frac{N_{pvs}}{N_{pvp}} R_{sh}}, & \text{(9a)} \\ f_{19} &= I_{ph} - N_{pvp} \times \\ &\left(\frac{R_{s} + R_{sh}}{R_{sh}} I_{sc,stc} + k_{I} \left(T_{c} - T_{c,stc} \right) \right) \frac{S}{S_{stc}}, & \text{(9b)} \\ f_{20} &= I_{0} - N_{pvp} \times \\ &\frac{I_{sc,stc} + k_{I} \left(T_{c} - T_{c,stc} \right)}{\exp(\frac{V_{oc,stc} + k_{V} \left(T_{c} - T_{c,stc} \right)}{n_{d} N_{s}} \frac{q}{K T_{c}}) - 1} & \text{(9c)} \end{split}$$

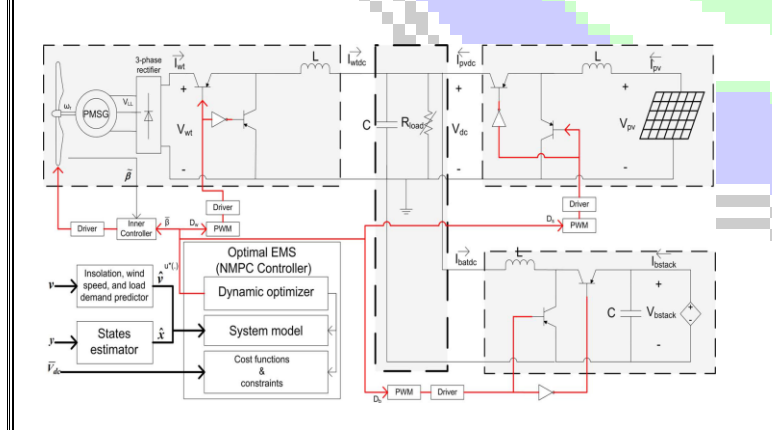


TABLE I
DESIGN PARAMETERS AND THE COMPUTATIONAL TIME
OF THE DEVELOPED NMPC CONTROLLER

Parameter Name	Parameter Value
Prediction horizon T (sec)	10
Sampling time h (sec)	5.0
No. of the discretization samples N	2
$\overline{V}_{dc}(V)$	48.0
Average Computational Time (sec)	2.066
Minimum Computational Time (sec)	0.628
Maximum Computational Time (sec)	3.565

The permissible deviation of the dc bus voltage level V_{dc} from the specified set point \overline{V}_{dc} is defined by a slack variable α_1 in (12). It is a design parameter set to $\pm 0.02\overline{V}_{dc}$ or equivalently ± 0.96 volt for a 48.0-volt dc bus:

$$f_{24} = \alpha_2 - \left\{ \frac{I_{wtdc} V_{dc}}{P_{wt,nom}} \left(\frac{U_{x,base}}{\max(U_x, U_{x,base})} \right)^3 - \frac{I_{pvdc} V_{dc}}{P_{nv,nom}} \frac{S_{x,base}}{\max(S_x, S_{x,base})} \right\}. \quad (13)$$

$$\begin{split} &J\left(\mathbf{x}(n),\mathbf{z}(n),\mathbf{u}(n),N\right) := \\ &\sum_{k=n}^{n+N} \left\{\beta_{1} \left\| \frac{1}{\overline{I}_{c}} \left(\frac{I_{bstack}(k)}{N_{batp}} - \overline{I}_{c} \right) \right\|_{2} + \beta_{2} \left\| \frac{V_{dc}(k) - \overline{V}_{dc}}{\overline{V}_{dc}} \right\|_{2} \right\} \\ &+ \left\{\beta_{1} \left\| \frac{1}{\overline{I}_{c}} \left(\frac{I_{bstack}(N)}{N_{batp}} - \overline{I}_{c} \right) \right\|_{2} + \beta_{2} \left\| \frac{V_{dc}(N) - \overline{V}_{dc}}{\overline{V}_{dc}} \right\|_{2} \right\}, \end{split}$$

$$J(\mathbf{x}(n), \mathbf{z}(n), \mathbf{u}(n), N) := \sum_{k=n}^{n+N} \left\{ \beta_3 \left\| \frac{V_{bstack}(k) - N_{bats} V_{gas}}{N_{bats} V_{gas}} \right\|_2 + \beta_4 \left\| \frac{V_{dc}(k) - \overline{V}_{dc}}{\overline{V}_{dc}} \right\|_2 \right\} + \left\{ \beta_3 \left\| \frac{V_{bstack}(N) - N_{bats} V_{gas}}{N_{bats} V_{gas}} \right\|_2 + \beta_4 \left\| \frac{V_{dc}(N) - \overline{V}_{dc}}{\overline{V}_{dc}} \right\|_2 \right\}.$$

$$(14)$$

When the battery voltage level is less than the gassing voltage, the proposed controller employs (14a) to charge the battery bank with the constant current \overline{I}_c . Once the battery voltage level exceeds the gassing voltage, the controller switches to (14b) to maintain it below the gassing voltage \overline{V}_{gas} and protect batteries from permanent damages. In order to prevent the dc bus voltage level from sticking at the upper or lower boundaries, the cost functions are defined as convex combinations of objectives with the weights $\beta_1 - \beta_4$. While β_1 and β_3 are close to 1.0, β_2 and β_4 are close to zero.

2) Box Constraints: Equation (15) adds the pitch angle control feature to the developed EMS in order to limit the produced aerodynamic power by the wind turbine [23]:

$$0 \le -T_e \omega_r \le P_{wt.nom}. \tag{15}$$

The other box constraints on the manipulated variables and the system states are formulated as follows:

$$x_{\min} \le x \le x_{\max},$$
 (16a)

$$u_{\min} \le u \le u_{\max}.$$
 (16b)

For instance, the duty cycles are limited between 20% and 80% and the pitch angle should be less than 30 degrees.

3) Initial Constraints: Prior to calculating the optimal solution over the next receding horizon, all system states, i.e., , as well as the dc bus voltage level are initialized by the measured or estimated values.

TABLE II Wind Turbine, PMSG, Battery Stack, and PV Parameters in This Study

Wind turbine		PMSG		Battery sta	ek	PV array	
$C_1(-)$	0.517	$J(Kg.m^2)$	0.35	$C_{max}(Ah)$	48.15	$R_s(\Omega)$	0.221
$C_2(-)$	116.0	F(N.m.s)	0.002	$R_{hat}(\Omega)$	0.019	$R_{sh}(\Omega)$	405.4
$C_3(-)$	0.4	P(-)	8	$V_0(V)$	12.3024	$n_d(-)$	1.3
$C_4(-)$	5.0	$\psi(V.s)$	0.8	$P_1(-)$	0.9	$N_s(-)$	54
$C_5(-)$	21.0	$P_{rated}(KW)$	10.0	$N_{bats}(-)$	8	$I_{sc,stc}(A)$	8.21
$C_6(-)$	0.007	$L_s(H)$	0.0083	$N_{batp}(-)$	3	$V_{oc,stc}(V)$	32.9
$\lambda_{opt}(-)$	8.1			$T_s(sec)$	0.726	$k_I(A/K)$	0.003
$P_{wt,nom}(KW)$	10.0			$V_{bstack,nom}(V)$	96.0	$k_V(V/K)$	-0.12
Rad (m)	4.01			$P_{bat,nom}(KW)$	1.296	$N_{pvs}(-)$	1
$U_{x,base}(m/s)$	12.0			$C_{10}(Ah)$	45.0	$N_{pvp}(-)$	10
$C_{p,max}(-)$	0.48			$V_{gas}(V)$	13.0	$P_{pv,nom}(KW)$	2.001

IV. RESULTS AND DISCUSSION

Table II shows the parameters of different components andtheir values in this study. The linear load demand is also lessthan or equal to 12 KW. Two test scenarios are carried out to evaluate the performance of the developed optimal EMS. Table III summarizes these test scenarios.

A. Scenario I: Constant Current Charging Mode

Fig. 4(a) illustrates the normalized wind speed, insolation, and load demand inputs to the system. Wind speed starts at the rating value of the generator and sharply increases by 37.5% at s. Load demand is below the nominal value, exceptbetween 300 to 600 s. Moreover, solar irradiance is constant during the simulation only for results clarification. Fig. 4(b)–(e) depicts the calculated optimal control variables. Applying these optimal control variables to standalone dc microgrid, different variables of the wind and solar branches are depicted in Fig. 5. Fig. 6 illustrates the resulting dc bus voltage and the battery bank SOC and charging currents. The wind branch operates at

MPPT mode up to secondswith a calculated pitch angle of zero as given in Fig. 4(b). Fig. 4(c) shows the calculated buck converter duty cycle that

adjusts the rotational speed of the wind turbine at its nomina value, as given by Fig. 5(a). Fig. 5(b) indicates that the resultingpower coefficient reaches to its maximum value.At and 600 s, the pitch angle goes up to 1.2 and 16 degrees, respectively, to promote pitching to feather [23]. Fig. 5(a) and (b) illustrates a combination of the speed and power coefficient variations that curtails the generation downto KW after s, as given by Fig. 5(e). Fig. 5(c) and (d) illustrates that though the PV array initially operates at its MPP, i.e., and, the controller curtails its generation down to KW [Fig. 5(f)] after s. Therefore, the power sharing deficiency in (13) is 0.035% which is within the permissible range of . It should be noted that causes a slight inaccuracy in the wind power generation which can be reduced by decreasing thedesign parameter. In spite of significant wind speed and load demand variations, Fig. 6(a) depicts that the dc bus voltage level stays within the npermissible range, i.e., . From Fig. 6(a), it can be seen that after s, when there is not enough generatedpower to charge battery, controller reduces the dc nbus voltage

Step1: Configurations

Set $\overline{\alpha}_1=0.02\overline{V}_{dc}$ and $\overline{\alpha}_2=0.01$; (slacks in Eqs. (12)-(13)) Set $T=10.0(sec),\ N=2$;

Instantiate an NLP solver;

Step 2: Measurements

Measure the states I_f , Q_{bat} , and ω_r values form the system;

Measure the dc bus voltage V_{dc} ;

Measure the battery stack voltage level V_{bstack} ;

Get the predicted wind speed, insolation, and load demand for the next 10 seconds from an external estimator;

Step 3: Constructing the OCP given by Eq. (11) using CasADi [34] $\mbox{IF } V_{bstack} < V_{gas} N_{bats} \mbox{ THEN}$

Use Eq. (14a) as the cost function; (constant current charging)

ELSE use Eq. (14b) as the cost function; (constant voltage charging)

Construct the vector \mathcal{F} (Eq. 11b) using functionals $f_1 - f_{24}$ (as in Eqs. (2)-(5), (7)-(10), and (12)-(13));

Apply the current and next step values of the wind speed, insolation, and load demand as the OCP parameters;

Construct Eq. (11g) from the box constraints defined by Eqs. (15)-(16) as well as two constraints $|\alpha_1| \leq \overline{\alpha}_1$ and $|\alpha_2| \leq \overline{\alpha}_2$;

Step 4: Initializations

Set the measured values of $I_f,\,Q_{bat},$ and ω_r as the initial values of differential states

Set the measured value of ${\cal V}_{dc}$ as the initial dc bus voltage value

Step 5: Discretization and solving the discretized problem

Discretize the OCP problem using the collocation method

Construct equivalent NLP problem

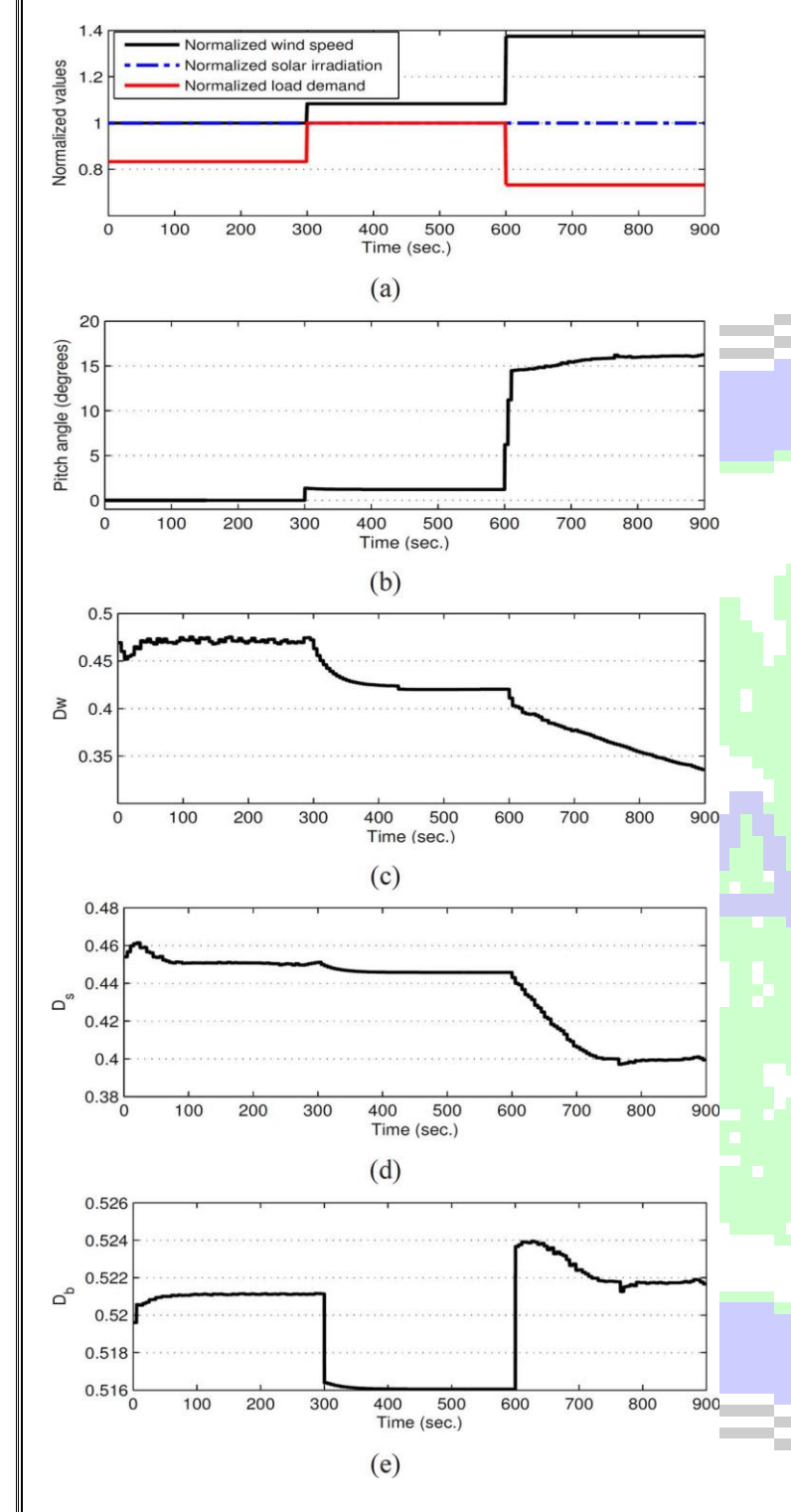
Solve the equivalent NLP problem using standard NLP solvers to calculate the optimal solution $u^{st}(.)$

Step 6: Applying the control variables

Constructing the control law using the first sample of the optimal solution, i.e. $u^*(0)$;

Apply the control law to the system

GOTO Step 2: Measurements;



V. CONCLUSION AND FUTURE WORKS

In this paper, we developed a novel optimal EMS that managesthe energy flows across a standalone green dc microgrid, consisting of the wind, solar, and battery branches. A coordinated and multivariable online NMPC strategy has been developed to address, as the optimal EMS, three main control objectives of standalone dc microgrids. These

objectives are thevoltage level regulation, proportional power sharing, and batterymanagement. In order to address these objectives, the developedEMS simultaneously controls the pitch angle of thewind turbine and the switching duty cycles of three dc-dc converters.

It has been shown that the developed controller tracksthe MPPs of the wind and solar branches within the normal conditionsand curtails their generations during the underload conditions. The provided flexible generation curtailment strategyrealizes the constant current-constant voltage charging regimethat potentially increases the life span of the battery bank. It isimportant to note that the proposed strategy can be employed as a centralized implementation of the primary and secondarylevels in the hierarchical architecture. The simulation resultshave shown its ability to achieve all control objectives. The issueof considering the discharging mode of the battery operation, which shifts the problem to the class of hybrid dynamical systems, is currently being investigated.

REFERENCES

[1] J. M. Guerrero, M. Chandorkar, T. Lee, and P. C. Loh, "Advanced Control Architectures for Intelligent Microgrids-Part I: Decentralized and Hierarchical Control," *IEEE Trans. Ind. Electron.*, vol. 60, no. 4, pp. 1254–1262, 2013.

[2] R. S. Balog, W. W. Weaver, and P. T. Krein, "The load as an energy asset in a distributed DC smartgrid architecture," *IEEE Trans. SmartvGrid*, vol. 3, no. 1, pp. 253–260, 2012.

[3] J. M. Guerrero, P. C. Loh, T. L. Lee, and M. Chandorkar, "AdvancedControl Architectures for Intelligent Microgrids-Part II: Power quality, energy storage, and AC/DC microgrids," *IEEE Trans. Ind. Electron.*, vol. 60, no. 4, pp. 1263–1270, 2013.

[4] N. Eghtedarpour and E. Farjah, "Control strategy for distributed integration

of photovoltaic and energy storage systems in DC microgrids," *Renew. Energy*, vol. 45, no. 0, pp. 96–110, 2012.

[5] D. Chen and L. Xu, "Autonomous DC voltage control of a DC microgrid

with multiple slack terminals," *IEEE Trans. Power Syst.*, vol. 27, no. 4, pp. 1897–1905, Nov. 2012.

[6] L. Xu and D. Chen, "Control and operation of a DC microgrid with a generation and energy storage," *IEEE Trans. Power Del.*, vol.26, no. 4, pp. 2513–2522, Oct. 2011.

[7] S. Anand, B. G. Fernandes, and M. Guerrero, "Distributed control toensure proportional load sharing and improve voltage regulation inlow-voltage DC microgrids," *IEEE Trans. Power Electro.*, vol. 28, no.4, pp. 1900–1913, 2013.

[8] B. Zhao, X. Zhang, J. Chen, C. Wang, and L. Guo, "Operation optimization of standalone microgrids considering lifetime characteristics of battery energy storage system," *IEEE Trans. Sustain. Energy*, to be published.

[9] T. Zhou and B. Francois, "Energy management and power control of ahybrid active wind generator for distributed power

generation and grid integration," *IEEE Trans. Ind. Electron.*, vol. 58, no. 1, pp. 95–104, 2011.

- [10] X. Liu, P. Wang, and P. C. Loh, "A hybrid AC/DC microgrid and its coordination control," *IEEE Trans. Smart Grid*, vol. 2, no. 2, pp. 278–286, 2011.
- [11] H. Kanchev, D. Lu, F. Colas, V. Lazarov, and B. Francois, "Energymanagement and operational planning of a microgrid with a PV-based active gen. for smart grid applications," *IEEE Trans. Ind. Electron.*,vol. 58, no. 10, pp. 4583–4592, 2011.
- [12] H. Ghoddami, M. B. Delghavi, and A. Yazdani, "An integrated windphotovoltaic-battery system with reduced power-electronic interface and fast control for grid-tied and off-grid applications," *Renew. Energy*, vol. 45, no. 0, pp. 128–137, 2012.
- [13] J. M. Guerrero, J. C. Vasquez, J. Matas, L. G. de Vicua, and M. Castilla,
- "Hierarchical control of droop-controlled AC and DC microgrids-ageneral approach toward standardization," *IEEE Trans. Ind. Electron.*, vol. 58, no. 1, pp. 158–172, 2011.
- [14] P. H. Divshali, A. Alimardani, S. H. Hosseinian, and M. Abedi, "Decentralized cooperative control strategy of microsources for stabilizing
- autonomous VSC-Based microgrids," *IEEE Trans. Power Syst.*, vol.27, no. 4, pp. 1949–1959, Nov. 2012.
- [15] P. C. Loh, D. Li, Y. K. Chai, and F. Blaabjerg, "Autonomous operation
- of hybrid microgrid with AC and DC subgrids," *IEEE Trans. PowerElectron.*, vol. 28, no. 5, pp. 2214–2223, 2013.
- [16] T. L. Vandoorn, B. Meersman, L. Degroote, B. Renders, and L. Vandevelde, "A control strategy for islanded microgrids with DC-Linkvoltage control," *IEEE Trans. Power Del.*, vol. 26, no. 2, pp. 703–713, Apr. 2011.